

 Open access • Journal Article • DOI:10.1093/MNRAS/STW2619

The dynamical environment of asteroid 21 Lutetia according to different internal models — [Source link](#)

Safwan Aljbaae, Safwan Aljbaae, T. G. G. Chanut, T. G. G. Chanut ...+4 more authors

Institutions: PSL Research University, Sao Paulo State University, National Institute for Space Research

Published on: 21 Jan 2017 - Monthly Notices of the Royal Astronomical Society (Oxford University Press)

Topics: Gravitational field, Displacement (vector), Position (vector) and Orbital motion

Related papers:

- [Exterior gravitation of a polyhedron derived and compared with harmonic and mascon gravitation representations of asteroid 4769 Castalia](#)
- [Analysis of the potential field and equilibrium points of irregular-shaped minor celestial bodies](#)
- [Orbits and manifolds near the equilibrium points around a rotating asteroid](#)
- [3D plausible orbital stability close to asteroid \(216\) Kleopatra](#)
- [3D stability orbits close to 433 Eros using an effective polyhedral model method](#)

Share this paper:    

View more about this paper here: <https://typeset.io/papers/the-dynamical-environment-of-asteroid-21-lutetia-according-23ivow5uuc>

The dynamical environment of asteroid 21 Lutetia according to different internal models

S. Aljbaae,^{1,2★} T. G. G. Chanut,^{1,3} V. Carruba,¹ J. Souchay,² A. F. B. A. Prado³
and A. Amarante¹

¹Univ. Estadual Paulista - UNESP, Grupo de Dinâmica Orbital & Planetologia, Guaratinguetá CEP 12516-410, Sao Paulo, Brazil

²SYRTE, Observatoire de Paris, PSL Research University, CNRS, Sorbonne Universités, UPMC Univ. Paris 06, LNE, 61 avenue de l'Observatoire, F-75014 Paris, France

³Division of Space Mechanics and Control, INPE, C.P. 515, 12227-310 São José dos Campos, Sao Paulo, Brazil

Accepted 2016 October 7. Received 2016 October 7; in original form 2016 September 13

ABSTRACT

One of the most accurate models currently used to represent the gravity field of irregular bodies is the polyhedral approach. In this model, the mass of the body is assumed to be homogeneous, which may not be true for a real object. The main goal of this paper is to study the dynamical effects induced by three different internal structures (uniform, three- and four-layered) of asteroid (21) Lutetia, an object that recent results from space probe suggest being at least partially differentiated. The Mascon gravity approach used in this work consists of dividing each tetrahedron into eight parts to calculate the gravitational field around the asteroid. The zero-velocity curves show that the greatest displacement of the equilibrium points occurs in the position of the $E4$ point for the four-layered structure and the smallest one occurs in the position of the $E3$ point for the three-layered structure. Moreover, stability against impact shows that the planar limit gets slightly closer to the body with the four-layered structure. We then investigated the stability of orbital motion in the equatorial plane of (21) Lutetia and propose numerical stability criteria to map the region of stable motions. Layered structures could stabilize orbits that were unstable in the homogeneous model.

Key words: gravitation – celestial mechanics – minor planets, asteroids: individual: (21) Lutetia.

1 INTRODUCTION

The main challenge for the navigators of space missions to small irregular bodies is to derive pre-mission plans for the control of the orbits. A lot of studies have already been focused on this issue (Scheeres 1994; Scheeres et al. 1998a,b; Rossi, Marzari & Farinella 1999; Hu 2002). Generally, the potential of an asteroid can be estimated from its shape assuming a homogeneous density distribution. Yet, it remains an approximation to reality, since real bodies are affected by density irregularities. Therefore, it seems worthwhile to discuss the effects of different mass distributions of objects on their gravity field and, consequently, on their orbital environment. For instance, several studies modelled the gravitational forces of Ceres and Vesta by a spherical harmonic expansion assuming diverse scenarios for interior structure (Tricarico & Sykes 2010; Konopliv et al. 2011, 2014; Park et al. 2014). In addition, the polyhedral approach (Werner & Scheeres 1997) seems more appropriate for evaluating the gravitational forces close to the surface. The main problem

of these approaches is the heavy computation time of the integrations. This issue has been reported in Rossi et al. (1999). Venditti (2013) developed a new approach that models the external gravitational field of irregular bodies through mascons. Recently, Chanut, Aljbaae & Carruba (2015a) also developed a mathematical model based on this approach. In this work we will use the approach of Chanut et al. (2015a), since we feel that it is more suitable for the studied problem. These authors applied the mascon gravity framework using a shaped polyhedral source, dividing each tetrahedron into up to three parts. That drives the attention to the possibility of taking into consideration the structure of layers in the gravitational potential computation.

The asteroid (21) Lutetia belongs to the main belt, the orbital space between Mars and Jupiter. An analysis of its surface composition and temperature, Coradini et al. (2011) showed that Lutetia was likely formed during the very early phases of the Solar system. Moreover, measurements by the European Space Agency's *Rosetta* have found that this asteroid was unusually dense for an asteroid (3.4 g cm^{-3}). Its large density suggests that the asteroid might be a partially differentiated body, with a dense metal-rich core (Pätzold et al. 2011; Weiss et al. 2012). For these reasons, (21) Lutetia

* E-mail: safwan.aljbaae@obspm.fr

represents a suitable object to test the effects of the layers structure on the gravity field.

Thus, this paper aims at computing the gravitational field associated with asteroid (21) Lutetia, considering a model with different density layers. Moreover, we mapped the orbital dynamics of a probe-target close to it, taking into account this inhomogeneous model. For these purposes, first the physical properties of the polyhedral shape of (21) Lutetia are presented in Section 2. Then, two models with different internal structures (three- and four-layered) are discussed in Section 3. Moreover, the dynamical properties in the vicinity of our target are studied in Section 4. Here, we calculated the Jacobi integral and obtained the zero-velocity surfaces and the particular solutions of the system. A numerical analysis of the stability of motions in the equatorial plane is presented in Section 5. Finally, the main results of our study are given in Section 6.

2 PHYSICAL PROPERTIES FROM THE POLYHEDRAL SHAPE OF LUTETIA WITH UNIFORM DENSITY

The relatively large asteroid (21) Lutetia is a primordial object, located in the inner part of the main-belt, with a perihelion of 2.036 au and an aphelion distance of 2.834 au. Its eccentricity (0.164) is moderate, and its inclination with respect to the ecliptical plane is quite small ($3^{\circ}.0648$) (Schulz et al. 2010). The asteroid was encountered by *Rosetta* spacecraft on its way to its final target (the comet 67P/Churyumov–Gerasimenko), at a distance of 3168 ± 7.5 km and a relative fly-by velocity of 14.99 km s^{-1} . The asteroid’s mass was estimated by the gravitational field distortion of the flyby trajectory measured by the Doppler shift of the radio signals from *Rosetta* as $(1.7 \pm 0.017) \times 10^{18}$ kg. It is lower than the previous estimation of $(2.59 \pm 0.24) \times 10^{18}$ kg obtained from asteroid to asteroid perturbations (Pätzold et al. 2011). Its bulk density of $3.4 \pm 0.3 \text{ g cm}^{-3}$ was calculated using the volume determined by the *Rosetta* Optical, Spectroscopic, and Infrared Remote Imaging System (OSIRIS) camera. This density is close to the density of M-type asteroids like (216) Kleopatra (Descamps et al. 2011).

Sierks et al. (2011) have modelled a global shape of (21) Lutetia, combining two techniques: stereo-photoclinometry (Gaskell et al. 2008) using images obtained by OSIRIS, and inversion of a set of 50 photometric light curves and contours of adaptive optics images (Carry et al. 2010; Kaasalainen 2011). 12 different shaped model solutions are listed in the Planetary Data System (PDS¹).

In this work, we selected the shape model that has 2962 faces from the PDS data base. The body is aligned with the principal axes of inertia, in such a way that the inertia tensor becomes a diagonal matrix. Thus, the x -axis is aligned with the smallest moment of inertia (longest axis), while the z -axis is aligned with the largest (shortest axis), and the y -axis is aligned with the intermediate one. The spin velocity of (21) Lutetia is assumed to be uniform around its maximum moment of inertia (z -axis) with a period of 8.168270 ± 0.000001 h (Carry et al. 2010). The algorithm of Werner (1997) was used to calculate the spherical harmonic coefficients $C_{n,m}$ and $S_{n,m}$ up to degree 4 (Table 1), considering a uniform bulk density of 3.4 g cm^{-3} . Please notice that these coefficients are presented as a reference for describing the exterior gravitational potential. They can be used to verify the orientation of our shape. If we fix the expansion of the gravitational field around the centre of mass, we have $C_{11} = S_{11} = 0$, and if the axes are exactly oriented along the principal axes of inertia, we have $C_{21} = S_{21} = S_{22} = 0$

Table 1. Lutetia Gravity Field Coefficients up to order 4, using the shape model of 2962 faces. These coefficients are computed with respect to a constant density of 3.4 g cm^{-3} , a total mass of 1.68×10^{18} kg (derived from the polyhedron volume), and a reference distance of 49.1 km.

Order	Degree	C_{nm}	S_{nm}
0	0	1.000 000 0000	–
1	0	$-2.416 144 5414 \times 10^{-16}$	–
1	1	$4.458 781 4343 \times 10^{-17}$	$7.214 010 2052 \times 10^{-17}$
2	0	$-1.304 730 3671 \times 10^{-1}$	–
2	1	$2.015 667 3639 \times 10^{-16}$	$8.948 733 6812 \times 10^{-17}$
2	2	$3.047 706 6056 \times 10^{-2}$	$8.652 170 5057 \times 10^{-16}$
3	0	$-8.122 587 5136 \times 10^{-3}$	–
3	1	$1.360 787 7846 \times 10^{-2}$	$6.437 744 7088 \times 10^{-3}$
3	2	$1.753 660 8648 \times 10^{-5}$	$-3.177 639 8240 \times 10^{-4}$
3	3	$-2.347 325 7023 \times 10^{-3}$	$1.599 494 9238 \times 10^{-3}$
4	0	$3.531 818 1727 \times 10^{-2}$	–
4	1	$8.152 203 8541 \times 10^{-4}$	$-4.767 014 1468 \times 10^{-3}$
4	2	$-2.492 682 1394 \times 10^{-3}$	$1.330 516 7431 \times 10^{-3}$
4	3	$3.825 676 4962 \times 10^{-5}$	$4.591 412 9725 \times 10^{-4}$

(Scheeres, Williams & Miller 2000). However, we did not use these coefficients in our analyses, our approach (mascon) employs the shape of the asteroid to calculate the exterior gravitational potential, which is more accurate than the harmonic coefficients even if this coefficients were measured up to a higher degree than four.

The algorithm of Mirtich (1996) provides these values of moments of inertia divided by the total mass of the body:

$$I_{xx}/M = 802.929 \text{ km}^2$$

$$I_{yy}/M = 1096.555 \text{ km}^2$$

$$I_{zz}/M = 1263.996 \text{ km}^2.$$

From the moments of inertia, we can solve for the equivalent ellipsoid according to Dobrovolskis (1996). The semimajor axes found are as follows: $62.402 \text{ km} \times 49.254 \text{ km} \times 39.859 \text{ km}$.

As discussed by Hu & Scheeres (2004), the main gravity coefficients are directly related to the principal moments of inertia (normalized by the body mass) and the unit is the distance squared.

$$C_{20} = -\frac{1}{2M}(2I_{zz} - I_{xx} - I_{yy}) = -314.254 \text{ km}^2$$

$$C_{22} = \frac{1}{4M}(I_{yy} - I_{xx}) = 73.406 \text{ km}^2.$$

A mass-distribution parameter σ can be determined to be the following:

$$\sigma = \frac{I_{yy} - I_{xx}}{I_{zz} - I_{xx}} = -\frac{4C_{22}}{C_{20} - 2C_{22}} = 0.637.$$

This value of σ denotes that Lutetia is not close to the rotational symmetry about the z -axis ($\sigma = 0$) or x -axis ($\sigma = 1$). That clearly appears in the elongated shapes viewed from various perspectives presented in Fig. 1, with overall dimensions (km) of $(-66.854, 57.959) \times (-54.395, 47.920) \times (-44.238, 39.721)$ in the x -, y -, and z -directions, respectively, and a polyhedral volume of $495 140.993 \text{ km}^3$ (volume-equivalent diameter of 98.155 km).

3 INTERNAL STRUCTURE OF LUTETIA

Because of its high *IRAS* albedo of 0.208 ± 0.025 , (21) Lutetia was classified as M-type asteroid by Barucci et al. (1987) and Tholen (1989). Analysing the visible spectrum, Bus & Binzel

¹ <http://sbn.psi.edu/pds/>

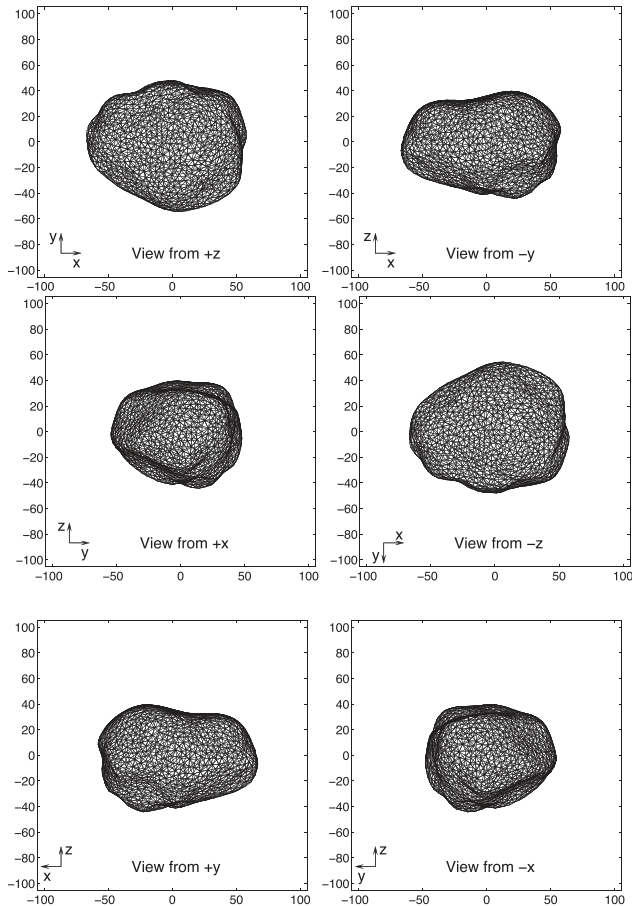


Figure 1. Polyhedral shape of (21) Lutetia shown in six perspective views ($\pm x$, $\pm y$, and $\pm z$), using the shape model provided by PDS data base with 2962 triangular faces (Sierks et al. 2011), after aligning the asteroid with the principal axes of inertia.

(2002) classified it as (Xk) on the basis of SMASS II spectroscopic data. Further spectroscopic observations by Birlan et al. (2004), Barucci et al. (2005), and Lazzarin et al. (2004, 2009) suggested a similarity with the carbonaceous chondrite spectra that characterize the C-type asteroids. Analysing the reflectance spectra, Busarev et al. (2004) indicated the possibility of Lutetia being an M-type body covered with irregular layer of hydrated silicates. The Bus-DeMeo taxonomy of asteroids (DeMeo et al. 2009) put Lutetia in the Xc subclass. Moreover, the available data from *ROSETTA* OSIRIS images have been analysed by Magrin et al. (2012) and compared consistently with ground-based observations, but no further deep analysis was possible, since *Rosetta* only made a relatively brief observation covering about 50 per cent of the surface.

According to Neumann, Breuer & Spohn (2013), (21) Lutetia may have a differentiated interior, i.e. an iron-rich core and a silicate mantle. Note that the other differentiated asteroid such as (1) Ceres and (4) Vesta have been visited by a spacecraft (*DAWN*). Because of its large diameter, we think that it is reasonable to expect an internal differentiated structure for (21) Lutetia as well. To understand the effects that such differentiation may have on the orbits of probes, we will study the dynamics in the vicinity of (21) Lutetia examining the effect of its inhomogeneity, considering two distinct models, based on a three-layered and a four-layered assumption, respectively, as already used for other differentiated objects.

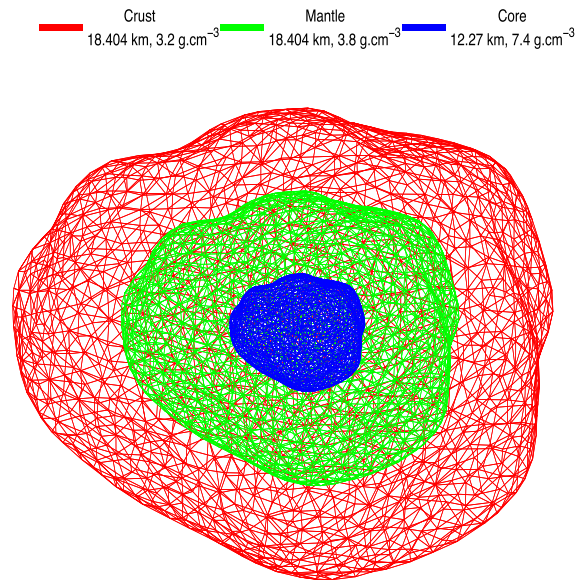


Figure 2. Three-layered structure of (21) Lutetia.

3.1 The three-layered internal model

Our three-layered model is similar to that discussed in Park et al. (2014) and Konopliv et al. (2014). It corresponds to a volume-equivalent diameter of 98.155 km, in which a crust with a mean thickness of 18.404 km occupies 75.59 per cent of the total volume with a density of 3.2 g cm^{-3} , that represents 71.06 per cent of the total mass. The mantle thickness of the asteroid is also modelled with a 18.404 km thickness (22.85 per cent of the total volume) and a density of 3.8 g cm^{-3} (25.54 per cent of the total mass). The core, based on iron meteorites characteristics, is considered with a 12.27 km thickness (1.56 per cent of the total volume) and a density of 7.4 g cm^{-3} (3.4 per cent of the total mass). This structure is exhibited in Fig. 2.

3.2 The four-layered internal model

A more sophisticated model of the internal structure of (21) Lutetia can be based on the model of Vesta discussed in Zuber et al. (2011). It consists in four layers, shown in Fig. 3. This model still includes an iron meteorite core with a thickness of 18.404 km (5.27 per cent of the total volume) and a density of 7.8 g cm^{-3} (12.1 per cent of the total mass). The mantle thickness is supposed to be 12.27 km (19.15 per cent of the total volume) with a density of 4.0 g cm^{-3} (22.52 per cent of the total mass). In that specific model, the crust itself is divided into an upper and lower layers with limits at, respectively, 12.27 and 6.13 km thickness. The upper crust represents 57.81 per cent of the total volume with a density of 2.86 g cm^{-3} (48.66 per cent of the total mass), whereas the lower crust represents 17.77 per cent of the total volume with a density of 3.2 g cm^{-3} (16.72 per cent of the total mass).

The two internal structures proposed for (21) Lutetia are summarized in Table 2. The layers size and density are constrained to the model of internal structures of Vesta discussed in Park et al. (2014), Konopliv et al. (2014), and Zuber et al. (2011). We preserve the total mass of Lutetia by fixing the medium density at 3.4 g cm^{-3} . In other words, the distribution of the gravity of Lutetia is changed in the three- and four-layered models to be greater at the centre, while the mean density is the same as in the uniform structure.

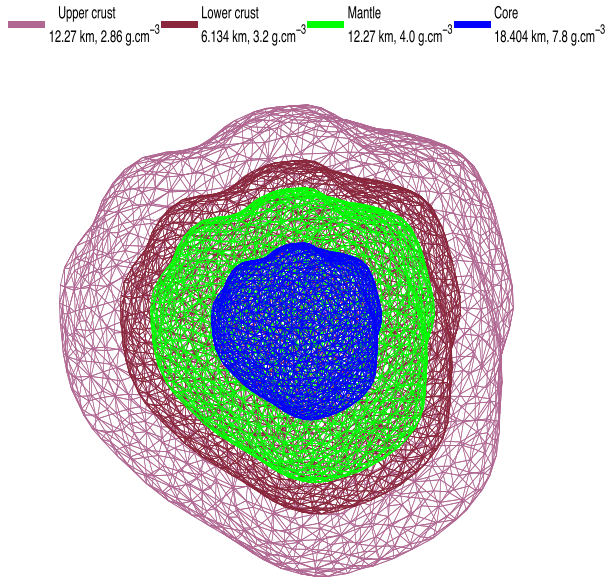


Figure 3. Four-layered structure of (21) Lutetia.

3.3 Influence of the internal models on the gravitational potential

For assessing the effects of the two different internal structures, described above, on the external potential of (21) Lutetia, we used the shape model with 2962 triangular faces and applied the approach of Chanut et al. (2015a), dividing each tetrahedron into up to eight parts (Mascon 8), to at 980 396 points placed in an equally spaced grid generated from the surface of the asteroid up to 200 km in the (x,y) plane. Mascon 8 seems to be satisfactory in terms of precision and computational time. Higher divisions could provide somewhat better accuracy but at a heavier computational cost.

Also, using the shape of the asteroid to model the external gravitational field according to the equation (9) in this paper or the equation (4) in Chanut et al. (2015a) is actually more accurate. According to Park et al. (2014), the spherical harmonic series may not converge close the surface, but the polyhedral approach is guaranteed to converge outside of the polyhedron.

In Fig. 4 (left-hand side), we present the relative difference of the gravitational potential considering a uniform density U_{M1} with the four-layered structure (red dots) or the three-layered structure (black dots). The figure shows that the relative difference is inversely proportional to the distance from the surface of the asteroid, and the potential calculated near the surface is affected significantly

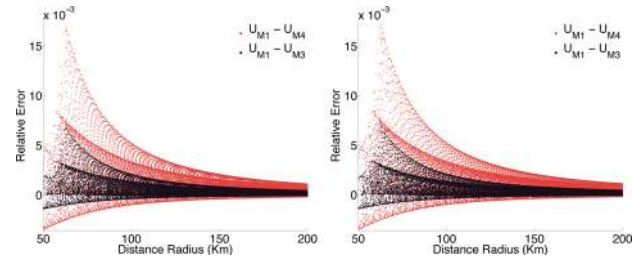


Figure 4. Relative difference of the gravitational potential calculated with Mascon 8 considering a uniform density U_{M1} with the model, considering a four-layered structure (red dots) or a three-layered structure (black dots), using the shape model with 11 954 triangular faces (left-hand side) and the shape model with 2962 triangular faces (right-hand side).

by the internal structure. Moreover, the shape model with 11 954 triangular faces is also used in this work to calculate the same relative difference, and presented in Fig. 4 (right-hand side). A very good agreement between the two shapes was found. In terms of CPU time, the total simulation time on a Pentium 3.8-GHz CPU took about 16 min using the first shape model, while required 54 min with the second one. That guided us to use the model with 2962 faces for the rest of this work.

4 EQUATIONS OF MOTION AND DYNAMICAL PROPERTIES IN THE VICINITY OF LUTETIA

In this section, we evaluate the dynamical environment close to (21) Lutetia caused by its in-homogeneous structure, and its consequences on any spacecraft orbiting around it. First, we consider a zone where the effect of the solar gravity is considerably smaller than the asteroid gravity, that is to say a region inside its Hill sphere. Its Hill radius $R_H = r_3 \sqrt{\frac{m}{3M_\odot}}$ varies between 20 042 km at perihelion (r_p) and 27 897 km at aphelion (r_a). As an example, within 300 km from the asteroid centre of mass, the solar gravity perturbation reaches $1.43 \times 10^{-12} \text{ m s}^{-2}$ at perihelion and $7.38 \times 10^{-13} \text{ m s}^{-2}$ at aphelion. That is completely negligible compared with the total gravitational attraction exercised by the asteroid on the spacecraft, which is $1.26 \times 10^{-6} \text{ km s}^{-2}$.

Another perturbation that arises from the Sun is the solar radiation pressure (SRP). Generally, the magnitude of the SRP acceleration (g) appears in the Hill equation of motion as a linear term in the first integral (Scheeres & Marzari 2002). Assuming that the spacecraft is a flat plate oriented to the Sun, the SRP acceleration g always

Table 2. Three- and four-layered structure of (21) Lutetia.

	Thickness (km)	Density (g cm^{-3})	Volume (per cent of the total volume)	Mass (per cent of the total mass)
Three-layered model				
Core	12.270	7.40	1.56	3.40
Mantle	18.404	3.80	22.85	25.54
Crust	18.404	3.20	75.59	71.06
Four-layered model				
Core	18.404	7.80	5.27	12.10
Mantle	12.27	4.00	19.15	22.52
Lower crust	6.13	3.20	17.77	16.72
Upper crust	12.27	2.86	57.81	48.66

acts in the antisolar direction. It is computed as follows:

$$g = \frac{\beta}{d^2}, \quad (1)$$

where $\beta = \frac{(1+\eta)G1}{B}$ is the SRP parameter, $G1 = 1 \times 10^8 \text{ kg km}^3 \text{ s}^{-2} \text{ m}^{-2}$ is the solar constant (Giancotti et al. 2014), η is the reflectance of the spacecraft material (equal to 0 for perfectly absorbing material and to 1 for perfect reflection), B is the spacecraft mass to area ratio in kg m^{-2} usually computed by dividing the total mass by the projected surface area of the spacecraft, and d is the heliocentric distance of the asteroid in kilometres. Taking into account the physical characteristics of a *Rosetta*-like spacecraft, i.e. a maximum projected area of 65 m^2 and a mass of 1400 kg (Scheeres et al. 1998a), the total SRP acceleration varies from 2.58×10^{-17} up to $5.00 \times 10^{-17} \text{ m s}^{-2}$ at the aphelion and perihelion distance from the Sun, respectively. After considering the above-given calculations, we neglect the effects of both the SRP and the solar gravity in our model.

4.1 Equations of motion

According to Scheeres et al. (1996) and Scheeres (1999, 2012), in the absence of any solar perturbations, the equations of motion of a spacecraft orbiting a uniformly rotating asteroid and significantly far from any other celestial body are

$$\ddot{x} - 2\omega\dot{y} = \omega^2 x + U_x \quad (2)$$

$$\ddot{y} + 2\omega\dot{x} = \omega^2 y + U_y \quad (3)$$

$$\ddot{z} = U_z, \quad (4)$$

where U_x , U_y , and U_z are the first-order partial derivatives of the potential $U(x, y, z)$, and ω is the spin rate of the asteroid.

Because equations (2) to (4) are time-invariant, the Jacobi constant exists as an additional integral of motion. The Jacobi integral for the equations of motion is conserved and is explicitly calculated as

$$C = \underbrace{\frac{1}{2}\omega^2(x^2 + y^2) + U(x, y, z)}_{\text{Modified potential}} - \underbrace{\frac{1}{2}(\dot{x}^2 + \dot{y}^2 + \dot{z}^2)}_{\text{Kinetic energy}}. \quad (5)$$

4.2 Zero-velocity surfaces and equilibria

As shown in equation (5), the Jacobi integral is a relation between the possible position of the particle and the kinetic energy with respect to the rotating asteroid. If the particle's velocity becomes zero, the zero-velocity surfaces are defined by

$$C = \frac{1}{2}\omega^2(x^2 + y^2) + U(x, y, z) = V(x, y, z), \quad (6)$$

where $V(x, y, z)$ is the modified potential.

This equation defines zero-velocity surfaces depending on the asteroid shape and also on the value of C . These surfaces are all evaluated close to the critical values of C and intersect or close in upon themselves at points called equilibrium points (Scheeres et al. 1996). The location of these equilibrium points can be found by solving the equation $\nabla V(x, y, z) = 0$. The number of solutions depends on the shape and on the spin rate of the asteroid.

Using the shape model of (21) Lutetia with 2962 triangular faces, the projection of the zero-velocity surface on to the $z = 0$ plane is shown in Fig. 5. The zero-velocity curves of the asteroid have four

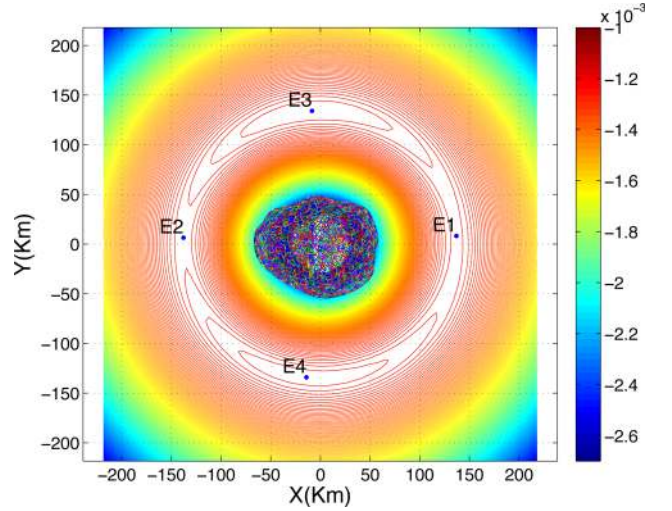


Figure 5. Zero-velocity curves and equilibrium points of (21) Lutetia in the x - y plane, obtained using the shape model with 2962 triangular faces and the four-layered structure. The colour code gives the intensity of the Jacobi constant in $\text{km}^2 \text{s}^{-2}$. The equilibrium points outside the body (E_1 , E_2 , E_3 , E_4) are displayed in the figure.

solutions outside the body, separated by approximately 90° in longitude. Only the external equilibria are presented in this work since there is not a good agreement between Mascon 8 and the classical polyhedron method inside the body. However, the agreement is better outside and near the body surface (Chanut et al. 2015a).

Fig. 5 displays the results from the Mascon 8 model and the four-layered structure. Results for the classical polyhedral model, for the Mascon 8 gravity model with uniform density, and for the Mascon 8 with three layers are similar and will not be displayed, for brevity. The maximum difference between the classical polyhedral approach and the Mascon 8, considering a uniform density, occurs at the location of E_4 (0.143 km, which represents 0.11 per cent of the distance from the centre of the body), and being less than the null hypothesis level, may therefore be considered satisfactory.

We observe that the positions of the equilibrium points (E_1 , E_2 , E_3 , E_4) are moved by up to 0.112, 0.137, 0.0614, and 0.143 km considering the three-layered structure, and up to 0.294, 0.351, 0.173, and 0.417 km considering the four-layered one, respectively.

As reported in many previous studies (Szebehely 1967; Scheeres 1994; Murray & Dermott 1999; Hu & Scheeres 2008; Yu & Baoyin 2012; Jiang et al. 2014; Wang, Jiang & Gong 2014), we can also examine the stability of the equilibria determined above. The linearized state equations in the neighbourhood of the equilibrium points are summarized as

$$\ddot{X} - 2\omega\dot{Y} + U_{xx}X + U_{xy}Y + U_{xz}Z = 0$$

$$\ddot{Y} + 2\omega\dot{X} + U_{xy}X + U_{yy}Y + U_{yz}Z = 0$$

$$\ddot{Z} + U_{xz}X + U_{xz}Y + U_{zz}Z = 0, \quad (7)$$

where $X = x - x_L$, $Y = y - y_L$, $Z = z - z_L$, and (x_L, y_L, z_L) denote the coordinates of the equilibrium point, $U_{\zeta\eta} = \frac{\partial^2 U}{\partial \zeta \partial \eta}$; $\zeta, \eta = x, y, z$. The eigenvalues of the equation (7) are calculated by finding the roots of the characteristic equation at the equilibrium point.

$$\lambda^6 + \alpha\lambda^4 + \beta\lambda^2 + \gamma = 0, \quad (8)$$

where λ are the eigenvalues, $\alpha = U_{xx} + U_{yy} + U_{zz} + 4\omega^2$, $\beta = U_{xx}U_{yy} + U_{yy}U_{zz} + U_{zz}U_{xx} - U_{xy}^2 - U_{yz}^2 - U_{xz}^2 + 4\omega^2U_{zz}$, $\gamma = U_{xx}U_{yy}U_{zz} + 2U_{xy}U_{yz}U_{xz} - U_{xx}U_{yz}^2 - U_{yy}U_{xz}^2 - U_{zz}U_{xy}^2$.

For more information, we recommend that interested readers review equation (14) in Jiang et al. (2014). The linearization method is applied using the classical polyhedral model and the Mascon 8 approach with uniform density and Mascon 8 gravity model considering the two multiple layered structures. This requires calculating the second derivatives of the potential that results in correcting the analytical form already presented in Chanut et al. (2015a) with the following expression:

$$U = \sum_{i=1}^n \frac{\mu_i}{r_i} \Rightarrow U_\zeta = \sum_{i=1}^n -\frac{\mu_i \zeta_i}{r_i^3}$$

$$\frac{\partial}{\partial \eta}(U_\zeta) = \sum_{i=1}^n \left[-\frac{\mu_i}{r_i^3} \frac{\partial}{\partial \eta}(\zeta_i) + \frac{3\mu_i \zeta_i \eta_i}{r_i^5} \right]. \quad (9)$$

Equation (7) leads to the second derivatives

$$U_{\zeta\zeta} = \sum_{i=1}^n \left[-\frac{\mu_i}{r_i^3} + \frac{3\mu_i \zeta_i^2}{r_i^5} \right]$$

$$U_{\zeta\eta} = \sum_{i=1}^n \left[\frac{3\mu_i \zeta_i \eta_i}{r_i^5} \right]$$

$$\zeta, \eta = x, y, z \text{ and } \zeta \neq \eta, \quad (10)$$

where $r = \sqrt{x^2 + y^2 + z^2}$ represents the distance between the centre of mass of each tetrahedron shaping the asteroid and the external

point. The eigenvalues of the linearized system are listed in Table 3. The classification of the equilibrium points is defined in Jiang et al. (2014); Wang et al. (2014) shows that $E1$ and $E2$ belong to Case 2 (two pairs of imaginary eigenvalues and one pair of real eigenvalues). As a consequence, the saddle equilibrium points are unstable, whereas $E3$ and $E4$ belong to Case 1 (purely imaginary eigenvalues), that leads to a linear stability of centre equilibrium points. Thus, according to the classification originally proposed by Scheeres (1994), (21) Lutetia can be classified as a type-I asteroid. We can conclude that the effects of the two-layered structures chosen on the stability of the equilibria are not determining.

5 ORBITAL STABILITY ABOUT LUTETIA

The goal of this section is to evaluate what should be the influence of Lutetia internal structure on the trajectory of a spacecraft in a close orbit. Thus, we numerically investigate the perturbations on initially equatorial orbits. In particular, we focus our analysis on the effects of the layered structures on limiting stability against impacts, so as to help us choosing the limits for periapsis radius in our stability analysis.

5.1 Stability against impact

According to Scheeres, Williams & Miller (2000), Chanut, Winter & Tsuchida (2014), and Chanut et al. (2015b), the stability

Table 3. Eigenvalues of the coefficient matrix at the four external equilibrium points.

Eigenvalues	$E1$	$E2$				$E3$		$E4$	
	($\times 10^{-3}$)	Tsoulis & Petrović (2001) considering the uniform density				(10 \times $^{-3}$)		(10 \times $^{-3}$)	
λ_1	0.220 401	i	0.225 039	i	0.215 898	i	0.217 647	i	
λ_2	-0.220 401	i	-0.225 039	i	-0.215 898	i	-0.217 647	i	
λ_3	0.217 889	i	0.223 367	i	0.186 893	i	0.195 130	i	
λ_4	-0.217 889	i	-0.223 367	i	-0.186 893	i	-0.195 130	i	
λ_5	-0.068 854		-0.096 044		0.098 844	i	0.076 583	i	
λ_6	0.068 854		0.096 044		-0.098 844	i	-0.076 583	i	
Mascon 8 considering the uniform densities									
	($\times 10^{-3}$)		(10 \times $^{-3}$)		(10 \times $^{-3}$)		(10 \times $^{-3}$)		(10 \times $^{-3}$)
λ_1	0.220 329	i	0.224 875	i	0.215 878	i	0.217 595	i	
λ_2	-0.220 329	i	-0.224 875	i	-0.215 878	i	-0.217 595	i	
λ_3	0.217 873	i	0.223 245	i	0.187 309	i	0.195 345	i	
λ_4	-0.217 873	i	-0.223 245	i	-0.187 309	i	-0.195 345	i	
λ_5	-0.068 571		-0.095 370		0.098 100	i	0.076 186	i	
λ_6	0.068 571		0.095 370		-0.098 100	i	-0.076 186	i	
Mascon 8 considering the three-layered structure									
	($\times 10^{-3}$)		(10 \times $^{-3}$)		(10 \times $^{-3}$)		(10 \times $^{-3}$)		(10 \times $^{-3}$)
λ_1	0.220 074	i	0.224 448	i	0.215 787	i	0.217 422	i	
λ_2	-0.220 074	i	-0.224 448	i	-0.215 787	i	-0.217 422	i	
λ_3	0.217 726	i	0.222 875	i	0.188 941	i	0.196 268	i	
λ_4	-0.217 726	i	-0.222 875	i	-0.188 941	i	-0.196 268	i	
λ_5	-0.067 270		-0.093 478		0.095 128	i	0.074 283	i	
λ_6	0.067 270		0.093 478		-0.095 128	i	-0.074 283	i	
Mascon 8 considering the four-layered structure									
	($\times 10^{-3}$)		(10 \times $^{-3}$)		(10 \times $^{-3}$)		(10 \times $^{-3}$)		(10 \times $^{-3}$)
λ_1	0.219 691	i	0.223 786	i	0.215 654	i	0.217 165	i	
λ_2	-0.219 691	i	-0.223 786	i	-0.215 654	i	-0.217 165	i	
λ_3	0.217 510	i	0.222 310	i	0.191 206	i	0.197 591	i	
λ_4	-0.217 510	i	-0.222 310	i	-0.191 206	i	-0.197 591	i	
λ_5	-0.065 291		-0.090 502		0.090 804	i	0.071 479	i	
λ_6	0.065 291		0.090 502		-0.090 804	i	-0.071 479	i	

Table 4. Locations of equilibrium points of (21) Lutetia and their Jacobi constant C (using the shape model of 2962 faces), generated by the classical polyhedral model (Tsoulis & Petrović 2001) and the Mascon 8 gravity model (Chanut et al. 2015a).

	x (km)	y (km)	z (km)	$C(\text{km}^2 \text{s}^{-2})$
Polyhedral model, uniform density				
$E1$	137.107 841 72	8.442 793 47	0.085 552 91	$-0.126\ 342\ 56 \times 10^{-2}$
$E2$	-138.191 443 78	6.565 513 58	0.041 856 44	$-0.126\ 799\ 36 \times 10^{-2}$
$E3$	-8.703 894 76	134.016 905 23	0.036 964 36	$-0.124\ 410\ 19 \times 10^{-2}$
$E4$	-14.618 312 74	-134.061 072 22	0.087 495 09	$-0.124\ 671\ 20 \times 10^{-2}$
Mascon 8, uniform density				
$E1$	137.087 698 19	8.389 608 64	0.090 771 55	$-0.126\ 326\ 87 \times 10^{-2}$
$E2$	-138.150 247 26	6.540 706 46	0.044 882 69	$-0.126\ 774\ 95 \times 10^{-2}$
$E3$	-8.664 586 28	134.028 112 12	0.038 544 83	$-0.124\ 415\ 17 \times 10^{-2}$
$E4$	-14.476 667 20	-134.075 451 74	0.093 705 61	$-0.124\ 671\ 57 \times 10^{-2}$
Mascon 8, three-layered structure				
$E1$	136.998 254 52	8.323 040 70	0.087 270 20	$-0.126\ 265\ 01 \times 10^{-2}$
$E2$	-138.015 474 66	6.508 022 98	0.043 227 24	$-0.126\ 692\ 15 \times 10^{-2}$
$E3$	-8.613 812 86	134.062 545 58	0.036 981 90	$-0.124\ 432\ 81 \times 10^{-2}$
$E4$	-14.334 588 20	-134.094 823 76	0.089 986 71	$-0.124\ 676\ 56 \times 10^{-2}$
Mascon 8, four-layered structure				
$E1$	136.867 070 31	8.195 207 30	0.080 685 57	$-0.126\ 173\ 28 \times 10^{-2}$
$E2$	-137.812 938 55	6.445 183 83	0.040 462 85	$-0.126\ 568\ 17 \times 10^{-2}$
$E3$	-8.515 699 13	134.115 225 33	0.034 338 57	$-0.124\ 459\ 11 \times 10^{-2}$
$E4$	-14.061 589 51	-134.129 209 61	0.083 188 37	$-0.124\ 683\ 67 \times 10^{-2}$

against impact is devoted to characterize the spacecraft dynamics, choosing initial conditions in such a way that the spacecraft stays in the outer portion of the zero-velocity curve, and the value of the Jacobi integral is smaller or equal to a specific value, corresponding to the minimum value of the Jacobi constant at the equilibrium point $E2$ listed in Table 4. A simple check in terms of osculating orbital elements (periapsis radius, eccentricity, and initial longitude) for an equatorial orbit is applied in order to determine the occurrence of an impact with the surface:

$$\frac{-\mu(1+e)}{2r_p} + W\sqrt{\mu r_p(1+e)} + U(r=r_p, \lambda) + J_0 = 0. \quad (11)$$

According to the last equation, the limits for the zones of stability against impact for Lutetia are shown in Fig. 6. The initial orbits that do not undergo impact with Lutetia correspond to the right-hand side of the curves. We remark that the curves related to the classical polyhedral approach and the Mascon 8 gravity model assuming a uniform density can hardly be distinguished. On the contrary, the curves related to multiple layered structures are quite distinct and get closer to the surface, which means that the non-impacting zones are larger than in the case of uniform density. The eccentricities in this analysis are limited to 0.4 because orbits with high eccentricities have a small perihelion distance, which implies that the spacecraft will travel at a high relative velocity when encountering the asteroid, and that would make these orbits unpractical for a space mission. We also notice that the initial eccentricity is not a primary parameter in affecting the periapsis distance: the periapsis distance is moved from a little less than 160 km for $e = 0.4$ to a little more than 175 km for $e = 0$. Thus, studying the stability against impact leads to conclude that orbits must lie outside of 175 km from Lutetia to avoid an impact on the surface.

5.2 Stability analysis

In this section, we present a numerical survey performed to find stable orbits around (21) Lutetia, with a period of 45 d, correspond-

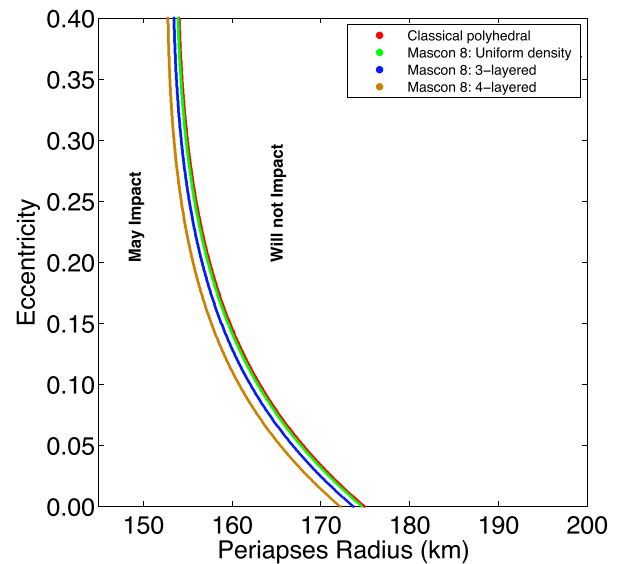


Figure 6. Stability against impact curve for equatorial, direct orbits around (21) Lutetia. The colours correspond to different approaches for calculating the potential: a classical polyhedral approach considering a uniform density and a Mascon 8 gravity model assuming the three- and four-layered structures shown in Table 2.

ing to more than 70 orbits around the asteroid. For this purpose, we consider the three different models of its internal structure. This work concentrates mainly on equatorial and prograde orbits. An orbit is considered stable if the oscillations of its eccentricity do not exceed a threshold value, although the orientation of these orbits may change. Thus, our task consists in observing the oscillation of $e(t)$ around its initial value. However, an alternative way for finding a stable orbits could be to measure oscillation in the periapsis radius instead of the oscillation of $e(t)$, that could be enhanced in future work. Following the previous section, orbits with a periapsis

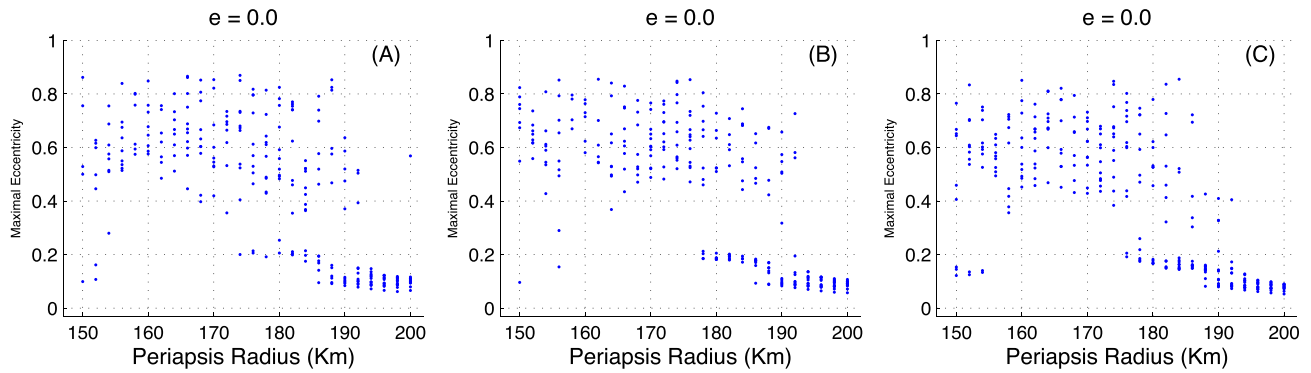


Figure 7. The maximal eccentricity of initially circular orbits about (21) Lutetia after 45 d, considering the one- (A), three- (B) and four-layered structure (C).

distance (r_p) between 150 and 200 km from the asteroid centre with an interval of 2 km are tested using the Bulirsch–Stoer integrator. We consider initially circular ($e_{\text{ini}} = 0$) or slightly eccentric orbits (with initial eccentricity of respectively 0.05, 0.1, and 0.2). For the sake of simplicity, initial conditions are chosen in such a way that each test particle is at the periapsis distance on the equatorial plane of the body ($i = 0$), with 12 different longitudes λ varying from 0° to 330° . Even with this discrete grid, a through exploration of the three-dimensional initial phase space (r_p, e, λ) requires 26 (periapsis radius) \times 4 (eccentricities) \times 12 (longitudes) = 1248 initial conditions for each model of the internal structure of Lutetia. The initial conditions in inertial space calculated from the two-body problem in the body-fixed reference frame are as follows:

$$\begin{aligned} x &= r_p \cos \lambda & \dot{x} &= - \left[\sqrt{\frac{\mu}{r}}(1+e) - r\omega \right] \sin \lambda \\ y &= r_p \sin \lambda & \dot{y} &= - \left[\sqrt{\frac{\mu}{r}}(1+e) - r\omega \right] \cos \lambda \\ z &= 0 & \dot{z} &= 0. \end{aligned}$$

The orbital position and velocity calculated in the rotating frame can then be transformed into position and velocity in the inertial frame with a simple approach. As already mentioned in the previous section, the new Mascon 8 approach, implemented by Chanut et al. (2015a) is chosen to calculate the gravitational field of the equations of motions in equations (2)–(4).

After eliminating orbits colliding with the body,² Fig. 7 shows the maximum eccentricities of initially circular orbits, after 45 d, considering the uniform (Fig. 7a), three-layered (Fig. 7b) and four-layered (Fig. 7c) structure of Lutetia. As a further general comment, one can notice that, within the considered area, no orbit escapes from the system. Nevertheless, a large majority of orbits suffer strong perturbations due to the irregular structure of Lutetia. An example of this behaviour can be seen in the three panels of Fig. 7. Objects starting with perfectly circular orbits experience changes in eccentricity of 0.06 after 45 d. These changes are not large enough to affect the stability of an eventual probe over the mission period, but could potentially be hazardous for longer time-scales. Interested

readers could find more information on results for orbits with larger initial eccentricities ($e_{\text{ini}} > 0$) in the appendix.

Despite similarities among different panels of Figs 7 and 8, a simple comparison of the three panels (a, b, and c) for each initial eccentricity shows that different internal structures of the asteroid could stabilize or destabilize some orbits. For initially eccentric orbits, (Fig. 8) shows an increase in the stability region when the initial eccentricity increases. Most important, for all the eccentricities here considered, the stability region increases when the three- and four-layered structures are considered.

Finally, in order to show the effects of the suggested core–mantle structure of (21) Lutetia on the orbital stability, three examples of 3D equatorial orbits after 45 d are displayed in Figs 9–11. The core–mantle structure can cause orbits to precess or regress around the asteroid, depending on the initial conditions. In the first examples (Fig. 9), considering the uniform structure destabilize the orbit, the orbit is destabilized considering three-layered structure in the second example. Finally, the four-layered structure stabilizes the orbit of the Fig. 11.

6 CONCLUSION

The computations carried out in this paper were performed based on the suggestion that the asteroid (21) Lutetia, the European space agency’s *Rosetta* mission target, may have an inhomogeneous density. This led to the problem of modelling its gravity field considering three different kinds of internal structures (uniform, three-layered and four-layered). Our different models of Lutetia structure were obtained within the Mascon gravity framework using the shaped polyhedral source, and dividing each tetrahedron into eight equal layers. The shape of Lutetia is presented, viewed from various perspectives after aligning the asteroid with the principal axes of inertia. The harmonic coefficients $C_{n,m}$ and $S_{n,m}$ up to degree 4, considering an uniform bulk density, were computed with respect to the reference radius. Then, two different internal structures for (21) Lutetia were considered to study the orbital dynamics in its vicinity and to examine the effect of the inhomogeneity. Both three-layered and four-layered Lutetia models provided important effects on the external potential. In their study of the gravity field, Vesta, Park et al. (2014) have shown that the thin crust model is the more appropriate representation of Vesta’s internal structure. In our case, the two-layered models provide a satisfactory estimation of the gravitational potential, within 150–200 km from the asteroid centre of mass, with a maximum relative difference from the uniform density equal to 9.38×10^{-4} . In terms of CPU time requirements, both

² As a first approximation, an ellipsoid with semimajor axes of 62.402 km \times 49.254 km \times 39.859 km is considered for detecting collisions. A more detailed study of every collisional event is, in our opinion, beyond the scope of this work.

of the models are somewhat comparable. However, a better close approach of a spacecraft is necessary to fit the real gravity data to find the plausible internal structure of this asteroid.

Correcting the analytical form of the second derivatives of the potential presented in Chanut et al. (2015a), we tested the stability of the equilibria points. We showed that the location of the equilibrium points can be slightly changed by up to 0.351 km. Moreover, the limiting planar figure of the stability against impact gets closer to the body considering the four-layered structure. Finally, in order to examine the potential effects of the inhomogeneity of Lutetia, stability analyses were investigated by testing orbits in an appropriate grid of initial conditions. Generally speaking, the stability region increases when considering the three- and four-layered structure. Future applications of this model could involve the study of the stability of polar orbits that are more suitable for mapping and reconnaissance purposes.

ACKNOWLEDGEMENTS

We are grateful to an anonymous referee for comments and suggestions that greatly improved the quality of this work. The authors wish to thank the São Paulo State Science Foundation (FAPESP), which supported this work via the grants 13/15357-1, 14/06762-2, 16/04476-8, and Brazilian National Research Council (CNPq) (grants 150360/2015-0, and 312313/2014-4).

REFERENCES

- Barucci M. A., Capria M. T., Coradini A., Fulchignoni M., 1987, *Icarus*, 72, 304
- Barucci M. A. et al., 2005, *A&A*, 430, 313
- Birlan M., Barucci M. A., Vernazza P., Fulchignoni M., Binzel R. P., Bus S. J., Belskaya I., Fornasier S., 2004, *New Astron.*, 9, 343
- Bus S. J., Binzel R. P., 2002, *Icarus*, 158, 146
- Busarev V. V., Bochkov V. V., Prokofeva V. V., Taran M. N., 2004, in Colangeli L., ed., *Astrophysics and Space Science Library*, Vol. 311, The New Rosetta Targets. Kluwer, Dordrecht, p. 79
- Carry B. et al., 2010, *A&A*, 523, A94
- Chanut T. G. G., Winter O. C., Tsuchida M., 2014, *MNRAS*, 438, 2672
- Chanut T. G. G., Aljbaae S., Carruba V., 2015a, *MNRAS*, 450, 374
- Chanut T. G. G., Winter O. C., Amarante A., Araújo N. C. S., 2015b, *MNRAS*, 452, 1316
- Coradini A. et al., 2011, *Science*, 334, 492
- DeMeo F. E., Binzel R. P., Slivan S. M., Bus S. J., 2009, *Icarus*, 202, 160
- Descamps P. et al., 2011, *Icarus*, 211, 1022
- Dobrovolskis A. R., 1996, *Icarus*, 124, 698
- Gaskell R. W. et al., 2008, *Meteorit. Planet. Sci.*, 43, 1049
- Giancotti M., Campagnola S., Tsuda Y., Kawaguchi J., 2014, *Celest. Mech. Dyn. Astron.*, 120, 269
- Hu W., 2002, PhD dissertation, Univ. Michigan
- Hu W., Scheeres D. J., 2004, *Planet. Space Sci.*, 52, 685
- Hu W.-D., Scheeres D. J., 2008, *Chin. J. Astron. Astrophys.*, 8, 108
- Jiang Y., Baoyin H., Li J., Li H., 2014, *Ap&SS*, 349, 83
- Kaasalainen M., 2011, *Inverse Probl. Imaging*, 5, 37
- Konopliv A. S., Asmar S. W., Bills B. G., Mastrodemos N., Park R. S., Raymond C. A., Smith D. E., Zuber M. T., 2011, *Space Sci. Rev.*, 163, 461
- Konopliv A. S. et al., 2014, *Icarus*, 240, 103
- Lazzarin M., Marchi S., Magrin S., Barbieri C., 2004, *A&A*, 425, L25
- Lazzarin M., Marchi S., Moroz L. V., Magrin S., 2009, *A&A*, 498, 307
- Magrin S. et al., 2012, *Planet. Space Sci.*, 66, 43
- Mirtich B., 1996, *J. Graph. Tools*, 1, 2
- Murray C. D., Dermott S. F., 1999, *Solar System Dynamics*. Cambridge Univ. Press, Cambridge
- Neumann W., Breuer D., Spohn T., 2013, *Icarus*, 224, 126
- Park R. S. et al., 2014, *Icarus*, 240, 118
- Pätzold M. et al., 2011, *Science*, 334, 491
- Rossi A., Marzari F., Farinella P., 1999, *Earth, Planets Space*, 51, 1173
- Scheeres D. J., 2012, *J. Guid. Control Dyn.*, 35, 987
- Scheeres D. J., 1994, *Icarus*, 110, 225
- Scheeres D. J., 1999, *J. Astronaut. Sci.*, 47, 25
- Scheeres D. J., Marzari F., 2002, *J. Astronaut. Sci.*, 50, 35
- Scheeres D. J., Ostro S. J., Hudson R. S., Werner R. A., 1996, *Icarus*, 121, 67
- Scheeres D. J., Marzari F., Tomasella L., Vanzani V., 1998a, *Planet. Space Sci.*, 46, 649
- Scheeres D. J., Ostro S. J., Hudson R. S., DeJong E. M., Suzuki S., 1998b, *Icarus*, 132, 53
- Scheeres D. J., Williams B. G., Miller J. K., 2000, *J. Guid. Control Dyn.*, 23, 466
- Schulz R., Accomazzo A., Küppers M., Schwehm G., Wirth K., 2010, European Planetary Science Congress, 2010, abstract #18
- Sierks H. et al., 2011, *Science*, 334, 487
- Szebehely V., 1967, *Theory of Orbits, The Restricted Problem of Three Bodies*. Academic Press, New York
- Tholen D., 1989, *Asteroids II*. Univ. Arizona Press, Tucson, AZ, p. 1139
- Tricarico P., Sykes M. V., 2010, *Planet. Space Sci.*, 58, 1516
- Tsoulis D., Petrović S., 2001, *Geophysics*, 66, 535
- Venditti V., 2013, PhD thesis, INPE, São José dos Campos
- Wang X., Jiang Y., Gong S., 2014, *Ap&SS*, 353, 105
- Weiss B. P. et al., 2012, *Planet. Space Sci.*, 66, 137
- Werner R. A., 1997, *Comput. Geosci.*, 23, 1071
- Werner R. A., Scheeres D. J., 1997, *Celest. Mech. Dyn. Astron.*, 65, 313
- Yu Y., Baoyin H., 2012, *AJ*, 143, 62
- Zuber M. T., McSween H. Y., Binzel R. P., Elkins-Tanton L. T., Konopliv A. S., Pieters C. M., Smith D. E., 2011, *Space Sci. Rev.*, 163, 77

SUPPORTING INFORMATION

Additional Supporting Information may be found in the online version of this article:

APPENDIX

(<http://www.mnras.oxfordjournals.org/lookup/suppl/doi:10.1093/mnras/stw2619/-/DC1>).

Please note: Oxford University Press is not responsible for the content or functionality of any supporting materials supplied by the authors. Any queries (other than missing material) should be directed to the corresponding author for the article.

This paper has been typeset from a $\text{\TeX}/\text{\LaTeX}$ file prepared by the author.